ADDENDUM IV: *AB INITIO CALCULATIONS ON THE CYCLIC THIOCARBONATE SYSTEM*

- *Introduction:*

It was observed experimentally[201], that upon homolytic fragmentation of a six-membered ring cyclic thionocarbonate attached to a five-membered ring, the formation of primary or secondary radicals could be controlled through the relative stereochemistry at the ring junction. When the ring junction was *trans*, the major product derived from the primary radical and when the ring junction was *cis* the major product derived from the secondary radical.

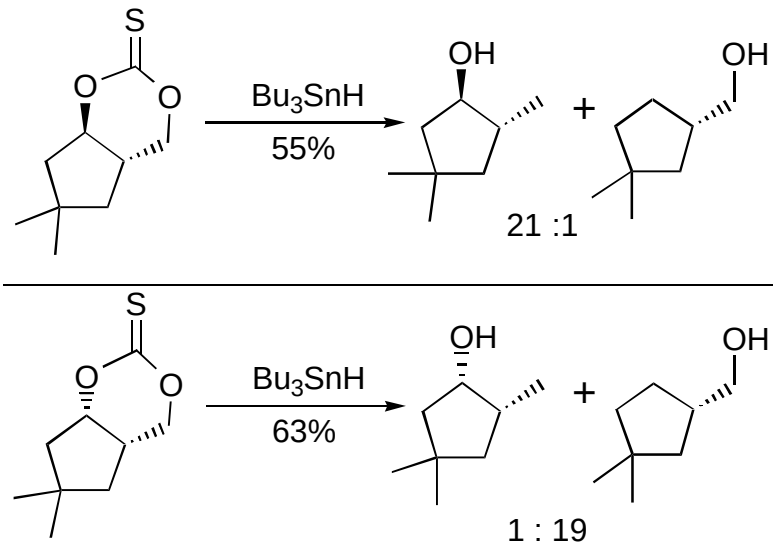

Figure IV.1

[201] (a) Ziegler, F. E.; Zheng, Z. L. *Tetrahedron Lett.* **1987**, *28*, 5973. (b) Ziegler, F. E.; Zheng, Z. L. *J. Org. Chem.* **1990**, *55*, 1416.

Ab initio calculations were used to address the question of whether the bond cleavage selectivity observed was due to thermodynamics and the stability of a specific intermediate, or due to other factors such as charge/spin distribution, ring strain release or orbital overlap.

Geometry calculations were conducted on a simplified version of the fragmentation system shown in Figure IV.1. Initially, a series of molecules was examined to determine if there was something inherently different about the 6-5-ring system (molecules **9** - **12**) *versus* a 6-6-ring system (molecules **7** - **10**) or a dimethyl substituted six-membered ring thionocarbonate (molecules **1** - **4**), in the context of *cis* versus *trans* substitution. Additionally, the effect of replacing sulfur with oxygen was explored in light of previous molecular mechanics studies[201] conducted in carbonates in order to clarify if there were fundamental differences in the thionocarbonate system's reactivity. Finally, the fragmentation reaction itself was examined starting from molecule **11**, representing the *cis* configuration and **12**, representing the *trans* configuration.

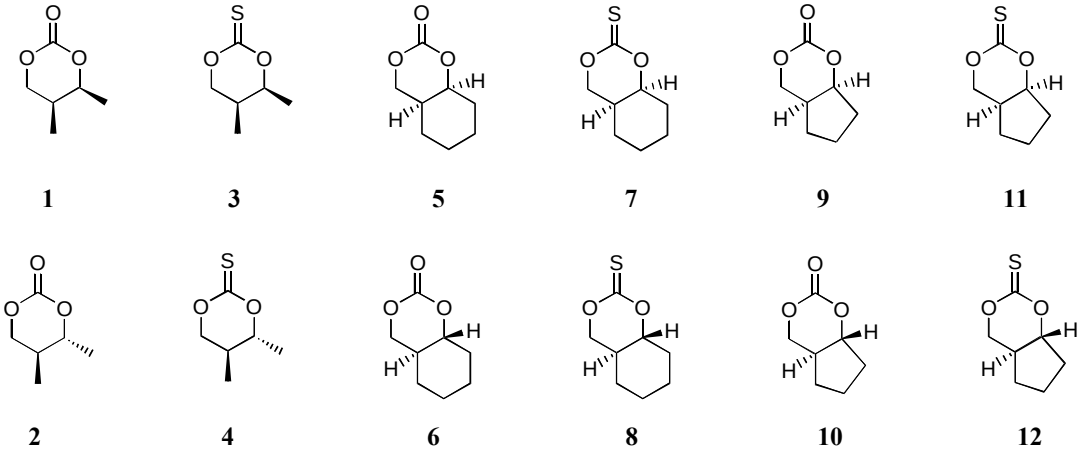

- *The ab initio procedure:*

The *ab initio* calculations were carried out using the software package Gaussian 94, Revision E.1[202]. Geometry calculations were conducted from an internally generated redundant internal coordinate system. Structures were fully optimized[203] at the RHF/6-31G* level[204] (as the highest level) for non-radical molecules and at the UHF/6-31G* level for radical molecules, using the Berny algorithm[205]. The geometries for the transition states were calculated using the Synchronous Transit-Guided Quasi-Newton (STQN) method. This method (keyword: QST3) uses a linear synchronous transit or quadratic synchronous transit approach to get closer to the quadratic region of the energy curve around the transition state, and then uses a quasi-Newton or eigenvector-following algorithm to complete the optimization. This generates a transition state structure that is midway between the reactants and products in terms of redundant internal coordinates, and then goes on to optimize this structure to a first-order saddle point. Assuming

---

[202] Gaussian 94, Revision E.1: M. J. Frisch, G. W. Trucks, H. B. Schlegel, P. M. W. Gill, B. G. Johnson, M. A. Robb, J. R. Cheeseman, T. Keith, G. A. Petersson, J. A. Montgomery, K. Raghavachari, M. A. Al-Laham, V. G. Zakrzewski, J. V. Ortiz, J. B. Foresman, J. Cioslowski, B. B. Stefanov, A. Nanayakkara, M. Challacombe, C. Y. Peng, P. Y. Ayala, W. Chen, M. W. Wong, J. L. Andres, E. S. Replogle, R. Gomperts, R. L. Martin, D. J. Fox, J. S. Binkley, D. J. Defrees, J. Baker, J. P. Stewart, M. Head-Gordon, C. Gonzalez, and J. A. Pople, Gaussian, Inc., Pittsburgh PA, 1995.

[203] Optimizations and vibrational frequency calculations used the analytical first and second derivative methods available with the Gaussian package.

[204] Basis set: 6-31G: Applies to: H-Cl. Polarization functions (3df,3pd). Diffuse functions ++.

[205] At each step of a Berny optimization the following actions are taken: The Hessian is updated; the trust radius (maximum allowed Newton-Raphson step) is updated if a minimum is sought, using the method of Fletcher; if a maximum is sought, the program performs a linear search between the latest point and the best previous point (the previous point having lowest energy). If the latest point is the best so far but if the newest point is not the best, the linear search must return a point in between the most recent and the best step to be acceptable. If all fits fail and the most recent step is the best so far, no linear step is taken. If all fits fail and the most recent step is not the best, the linear step is taken to the midpoint of the line connecting the most recent and the best previous points. Finally, convergence is tested against criteria for

stretching of the bonds involved in the cleavage provided an initial guess for the transition state in these calculations. The calculations were conducted from reagent to product and vice versa with the same results.

Following geometry calculations, frequency analyses were conducted in order to make sure the geometry obtained corresponded to a stable geometry (a minimum for the ground state or a maximum for the transition state). The frequency keyword computes force constants and the resulting vibrational frequencies and their intensities. The force constants were determined analytically whenever possible. The default is to use 298.15 K, 1 atmosphere, and the most abundant isotopes. Unscaled vibrational frequencies for all species were used to characterize stationary points. Each of the ground state structures had no negative eigenvalues and the transition structures had just one negative eigenvalue of the Hessian matrix.

The radicals were also submitted to a stability calculation (keyword: stable) to test the stability of the Hartree-Fock wavefunction. This was accomplished by computing the wavefunction as usual and then verifying if the resulting determinant of the Hessian matrix was a local minimum with the specified number of degrees of freedom. In examining the results prior to a frequency calculation, it sufficed to determine if any singlet instabilities existed for a restricted wavefunction (singlet state molecule) or if any singlet or triplet instability existed for an unrestricted wavefunction (radical).

---

the maximum force component, root-mean-square force, maximum step component, and root-mean-square step. The step is the change between the most recent point and the next to be computed.

Analysis of the calculations utilized the following information: energy[206], charge distribution and geometry. Additionally, the deviation from the ideal angle associated with each molecule or parts of the molecule was evaluated by examining the displacement from the minimized calculated structure to the ideal geometry for each atom as a means of evaluating the bend-angle-strain associated with different portions of the molecule. The strain associated with a molecule has six components, angle strain, torsion strain, strain associated with bond stretching, a cross term that associates stretching with bending, electrostatic interactions and Van der Waals forces. The angle strain portion of the strain was considered important in determining the outcome of the reaction and the one that varied the most throughout the reaction process. A formula was developed (Eq. 1) for qualitatively examining the angle displacement at each atom position in a molecule. This representation of angle displacement was denoted the "offset" and represents a number from 0-1, in which an offset of 0 means the minimized geometry of the molecule is close to the ideal angle distribution and 1 means the maximum possible offset associated with that atom. This offset value could be used to evaluate the ideal angle displacement for the entire molecule or for specific parts of the molecule. This was accomplished by summing the offset on all atoms involved in the region of the molecule being studied.

The offset for an atom was calculated by summing the square of the normalized difference between the energy minimized angle and the ideal hybridization angle (109.6 degrees for an sp^3 center or 120 degrees for an sp^2 center) over all angles involving the atom, then diving by the number of angles.

---

[206] 1 Hartree equals 627.5095 Kcal/mol

$$(1) \qquad offset = \frac{\sum_{i=1}^{N} \left[\left(\theta^{hyb} - \theta_i^{calc} \right) / \theta^{hyb} \right]^2}{N} \qquad \begin{array}{l} \text{for } sp^3 \text{ atom, } ideal\_angle = 109.6^o \\ \text{for } sp^2 \text{ atom, } ideal\_angle = 120^o \end{array} \qquad \text{Eq. 1}$$

Where N is defined as the number of angles involving the atom, θ^{hyb} is the ideal hybridization angle, and θ^{calc} is the calculated angle from the energy-minimized geometry.

- *Sample calculation:*

The steps involved in the calculation of the geometry, frequency and offset-from-the-ideal-angle for the *cis*-dimethyl-carbonate molecule (**1**) are shown below as an example of how these calculations were conducted. First, the actual Gaussian 94 input file for the geometry calculation is displayed; the other Gaussian input files are very similar and will not be shown. Second, summarized results extracted from the Gaussian output "log" files for each calculation are presented. The geometry information obtained by the calculation was transformed into a Protein Data Bank (pdb) file, using the perl script gaussian2pdb.pl, for ease of display. The offset-from-the-ideal-angle was calculated as discussed above by the script angle_strain.pl and the script sum_angle_strain.pl. The angle_strain.pl script creates a text file that can be used along with the pdb file to show the offset-from-the-ideal-angle graphically, as in the drawing in Figure IV.2 (generated using

the Raswin Molecular Graphics[207] package). A similar graphical representation was generated for the display of the charge or spin distribution in the molecule by using the script get_charge.pl.

1. Cis dimethyl carbonate Geometry calculation input file:

```
%chk=ciscarb.chk
%mem=32MB
#P RHF/6-31G* OPT MINPOP

Cis-dimethyl-carbonate geometry calculation

0    1
C
C    1     R2
H    1     R3          2     A3
H    1     R4          2     A4          3     D4          0
H    1     R5          2     A5          3     D5          0
C    2     R6          1     A6          3     D6          0
C    2     R7          1     A7          6     D7          0
H    2     R8          1     A8          6     D8          0
C    6     R9          2     A9          1     D9          0
O    6     R10         2     A10         9     D10         0
O    7     R11         2     A11         1     D11         0
H    6     R12         2     A12         9     D12         0
H    7     R13         2     A13         11    D13         0
H    7     R14         2     A14         11    D14         0
C    10    R15         6     A15         2     D15         0
H    9     R16         6     A16         2     D16         0
H    9     R17         6     A17         16    D17         0
H    9     R18         6     A18         16    D18         0
O    15    R19         10    A19         6     D19         0

R2  =1.5360587
R3  =1.0839627
R4  =1.08196533
R5  =1.08130809
R6  =1.53075197
R7  =1.52752278
R8  =1.08384576
R9  =1.5198039
R10 =1.46029031
R11 =1.45263248
R12 =1.08312181
R13 =1.07692785
R14 =1.0817535
R15 =1.3532833
R16 =1.08166351
R17 =1.0801125
R18 =1.08376274
R19 =1.18917366
A3  = 110.13106118
A4  = 111.30292678
A5  = 110.62137288
A6  = 112.89088224
```

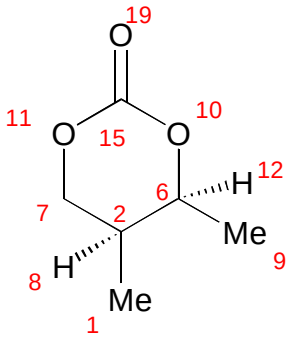

[207] Raswin Molecular Graphics, Windows version 2.6 copyright 1993-1995 R. Sayle, Freeware for molecule visualization downloaded from *http://www.umass.edu/microbio/rasmol*.

```
A7  = 110.90441927
A8  = 110.16877285
A9  = 116.30528266
A10 = 108.71166244
A11 = 110.45216377
A12 = 108.82965216
A13 = 112.42634479
A14 = 110.9286429
A15 = 124.0691475
A16 = 109.27422745
A17 = 110.27567666
A18 = 110.36390674
A19 = 121.96874819
D4  = 119.59575808
D5  =-119.65962609
D6  = 174.55270722
D7  =-118.41023285
D8  = 121.53172655
D9  =  54.46795479
D10 =-118.56875632
D11 =  67.39270586
D12 = 124.56563236
D13 =-117.11771105
D14 = 120.06834693
D15 = -39.00116566
D16 = 179.1315627
D17 = 118.78225922
D18 =-119.9774802
D19 = 190.98539747
```

2. Geometry calculation Results:

Note: HF represents the energy in Hartree units, 1 HF equals 627.5095 Kcal/mol.

G94 - tecate
#P RHF/6-31G* OPT MINPOP
Job CPU time: 9 hours 12 minutes 48.9 seconds.

HF = -457.6374734

Charge distribution

```
  1 C   -0.493262
  2 C   -0.255991
  3 H    0.175311
  4 H   0.179731
  5 H   0.190925
  6 C   0.166100
  7 C   0.007118
  8 H   0.188240
  9 C   -0.490711
 10 O   -0.634657
 11 O   -0.622637
 12 H   0.180208
 13 H   0.202712
 14 H   0.182263
 15 C   1.027624
 16 H   0.195730
 17 H   0.188378
 18 H   0.165337
 19 O   -0.552418
 Sum of Mulliken charges = 0.00000
```

3. Frequency calculation Results:

G94 - tecate

#P RHF/6-31G* FREQ MINPOP
Job CPU time: 0 days 10 hours 56 minutes 35.4 seconds.

NImag=0

4. Geometry pdb file:

```
REMARK Cisdimethylcarbonate geometry calculation.
ATOM      1    C                 0.882  -1.117  -1.582
ATOM      2    C                 0.853  -1.066  -0.051
ATOM      3    H                 1.908  -1.129  -1.935
ATOM      4    H                 0.398  -2.010  -1.956
ATOM      5    H                 0.391  -0.259  -2.026
ATOM      6    C                -0.542  -0.937   0.552
ATOM      7    C                 1.631   0.115   0.501
ATOM      8    H                 1.304  -1.973   0.342
ATOM      9    C                -1.575  -1.945   0.090
ATOM     10    O                -1.078   0.352   0.250
ATOM     11    O                 0.967   1.340   0.236
ATOM     12    H                -0.451  -1.000   1.632
ATOM     13    H                 2.606   0.216   0.047
ATOM     14    H                 1.761   0.025   1.574
ATOM     15    C                -0.353   1.461   0.182
ATOM     16    H                -2.507  -1.784   0.618
ATOM     17    H                -1.769  -1.849  -0.971
ATOM     18    H                -1.232  -2.954   0.296
ATOM     19    O                -0.862   2.514   0.044
CONECT    1    2    3    4    5
CONECT    2    1    6    7    8
CONECT    3    1
CONECT    4    1
CONECT    5    1
CONECT    6    2    9   10   12
CONECT    7    2   11   13   14
CONECT    8    2
CONECT    9    6   16   17   18
CONECT   10    6   15
CONECT   11    7   15
CONECT   12    6
CONECT   13    7
CONECT   14    7
CONECT   15   10   11   19
CONECT   16    9
CONECT   17    9
CONECT   18    9
CONECT   19   15
END
```

5. Calculated Offset-from-the-ideal-angle:

```
Atom number 1 with hybridization sp3 and total strain percentage 0.0268
Atom number 2 with hybridization sp3 and total strain percentage 0.0826
Atom number 6 with hybridization sp3 and total strain percentage 0.0937
Atom number 7 with hybridization sp3 and total strain percentage 0.0482
Atom number 9 with hybridization sp3 and total strain percentage 0.0092
Atom number 10 with hybridization sp3 and total strain percentage 0.2630
Atom number 11 with hybridization sp3 and total strain percentage 0.2180
Atom number 15 with hybridization sp2 and total strain percentage 0.0172

Total conformation strain percent is 0.7587
Total carbonate ring strain percent is 0.7227
Total strain per atom is 0.0948
```

6. Graphical representation:

The graphics in Figure IV.2 were generated using the angle_strain.pl and get_charge.pl scripts respectively to generate scripts that were overlaid on top of the pdb file using the Raswin graphical display package.

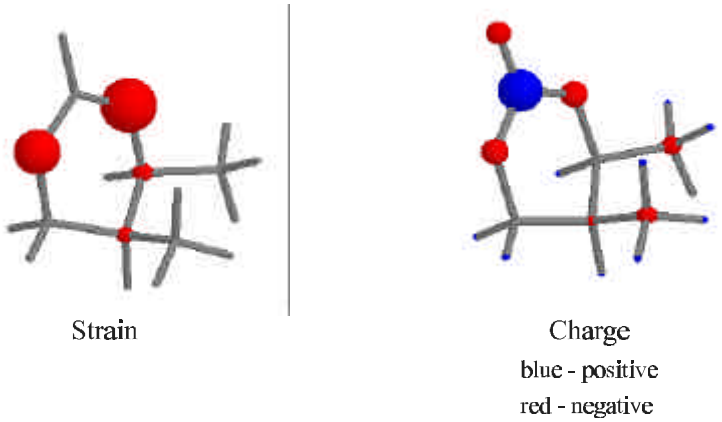

Figure 2: Offset-from-the-ideal-Angle and charge distribution for molecule 1

- *Results: Substituent effects on the carbonate ring:*

Analysis of the effect of substituents on the carbonate ring showed no significant or unexpected difference in energy between the *cis* and the *trans* series (**1** and **2**, **3** and **4**, **5** and **6**, etc).

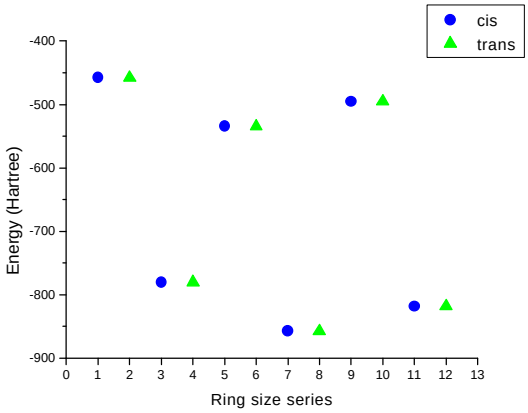

Compound Number	Energy (Hartree) ab initio	Energy (Kcal/mol) MacroModel
1	-457,6375	17,8200
2	-457,6393	17,0400
3	-780,2564	8,5300
4	-780,2582	19,3100
5	-534,5498	21,3400
6	-534,5501	20,3900
7	-857,1689	12,0100
8	-857,1689	23,0100
9	-495,5063	26,0000
10	-495,4997	27,0800
11	-818,1251	23,3100
12	-818,1182	29,7400

Figure IV.3

The energies for these molecules were also calculated using a molecular mechanics methodology with the software package MacroModel. The results from these energy calculations show striking differences between the *cis* and *trans* thiocarbonates pairs (**3** and **4**, **7** and **8**, **11** and **12**), in contrast to the *ab initio* results. This may be attributed to imprecise parameters for calculations involving sulfur atoms or cyclic carbonate and thiocarbonates available with the MM2 package. Figure IV.3 shows a table comparing the results of the *ab initio* and molecular mechanics calculations.

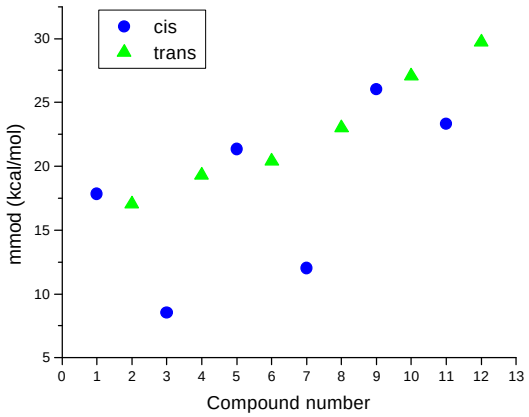

Analysis of charge distribution on the molecules demonstrated that there was very little difference within the series. The trend was that the carbon of the carbonate is positive and the oxygens are negative. There is a larger charge separation for the carbonates when compared to the thionocarbonates.

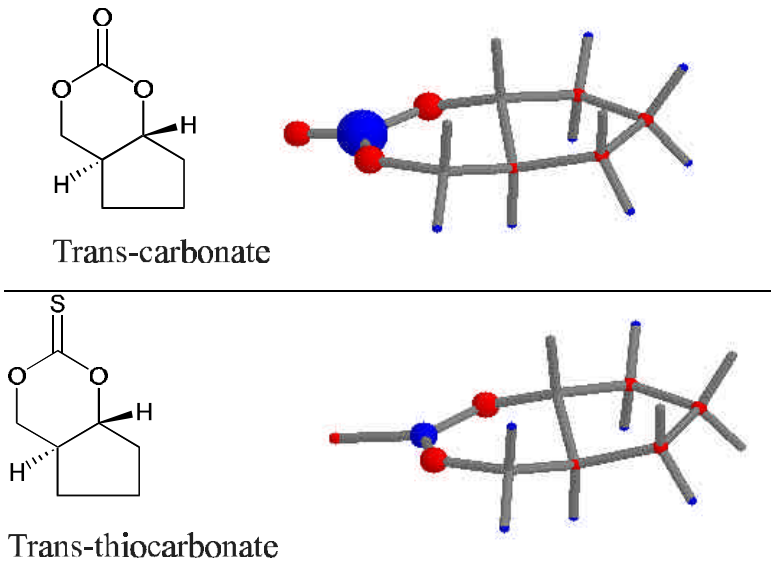

Figure IV.4: carbonate *vs* thiocarbonate charge distribution. Red is negative charge, blue is positive.

The stereochemistry at the ring junction is important in defining the geometrical conformations of the molecules; the *cis* molecules adopted different conformations from the *trans* molecules, as would be expected. The carbonate and thionocarbonate isomer pairs adopted very similar conformations in the 6-6 and dimethyl systems. However, the *cis* compound in the 6-5 ring series carbonate and thiocarbonate (**9** and **11**) adopted different conformations, as shown in Figure IV.5.

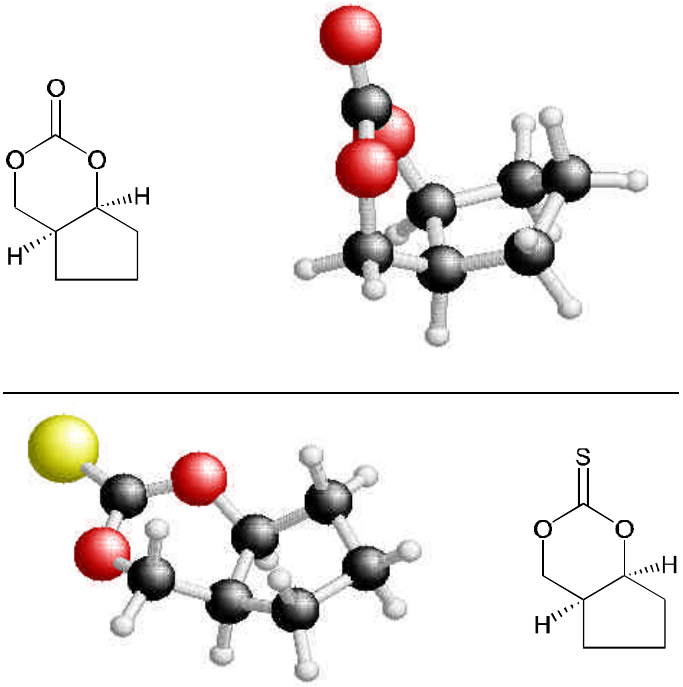

Figure IV.5: Geometry differences in the *cis* 6-5 ring series

Analysis of the distribution of offset-from-the-ideal-angle showed that, unlike the 6-6 system (**5**, **6**, **7**, **8**) and the dimethyl series (**1**, **2**, **3**, **4**), the 6-5 series shows a large difference between the *cis* and the *trans* isomers. The *trans* molecules in the 6-5-ring series (**10, 12**) present a higher offset-from-the-ideal-angle than the *cis* compounds (**9, 11**)

and the *cis* thionocarbonate **11** show less offset-from-the-ideal-angle than its carbonate **9** counterpart. These trends were observed when analyzing the total-offset, the offset-per-atom and the carbonate-offset. Analysis of the ring offset showed a larger offset associated with the five-membered ring (**9**, **10**, **11**, **12**) than the six-membered ring (**5**, **6**, **7**, **8**), but it also showed a larger offset associated with the *trans* compounds **10** and **12** than with the *cis* (**9**, **11**).

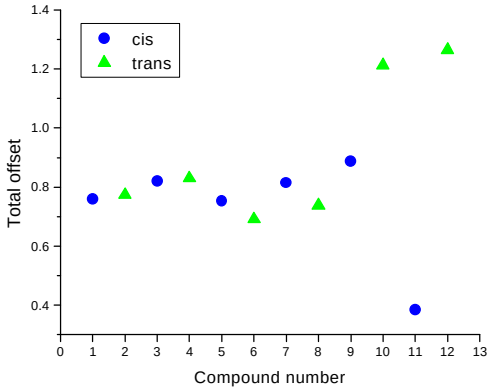

Compound Number	Total Offset	Ring Offset	carbonate Offset	per atom Offset
1	0.7587		0.7227	0.0948
2	0.7741		0.7404	0.0968
3	0.8198		0.7847	0.1025
4	0.8298		0.7979	0.1037
5	0.7533	0.1725	0.6740	0.0753
6	0.6915	0.1341	0.6247	0.0692
7	0.8147	0.1856	0.7341	0.0815
8	0.7375	0.1398	0.6713	0.0738
9	0.8878	0.3824	0.6701	0.0986
10	1.2122	0.5872	0.9816	0.1347
11	0.3847	0.3847	0.2837	0.0427
12	1.2646	0.5961	1.0319	0.1405

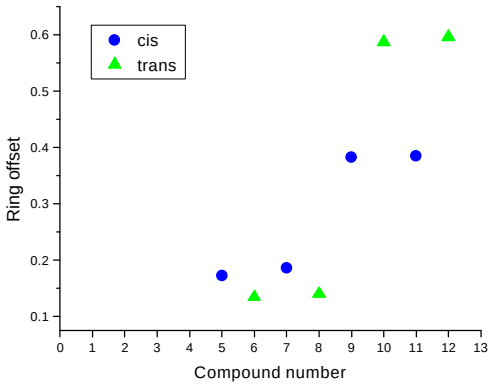

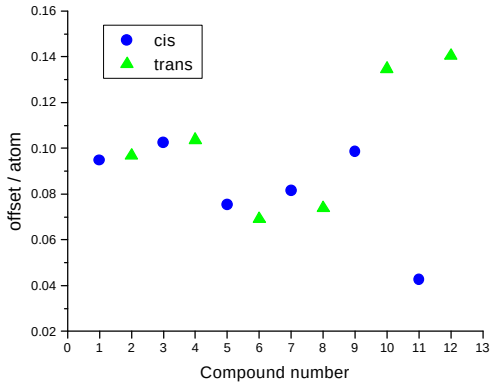

Figure IV.6

The offset-from-the-ideal-angle is slightly larger for the thionocarbonates (**3, 4, 7, and 8**) than the respective carbonates (**1, 2, 5, and 6**) in the dimethyl and 6-6 series. The offset-from-the-ideal-angle is larger for the *trans* thiocarbonate (**12**) than the carbonate counterpart (**10**) in the 6-5 series, while the opposite is true for the *cis* compounds (**11** and **9**).

To conclude, the *ab initio* studies on this series of molecules demonstrated that *cis* and *trans* molecules have similar energies. The molecular mechanics methods do not accurately model these systems and should be avoided, this is probably because they do not model the cyclic thionocarbonates well. The charge distribution results indicated that it does not contribute to the selectivity. The offset-from-the-ideal-angle calculations showed a difference between the thionocarbonates when compared to the carbonates, especially in the 6-5 series.

- *Results: Fragmentation reaction - cis:*

The fragmentation of a cyclic thionocarbonate was examined applying *ab initio* calculations using the methods described in "the *ab initio* procedure" section. The *cis* thionocarbonate fragmentation is examined in this section. The scheme below shows the two possible reaction pathways *via* bond cleavage to give a primary radical (**19**) or a secondary radical (**21**). Experimentally, its been shown that the fragmentation of a *cis* 6-5 system (represented here by compound **11**) gave rise to the product derived from a secondary radical (represented here by compound **29**) as the preferred pathway for the reaction (see Figure IV.1).

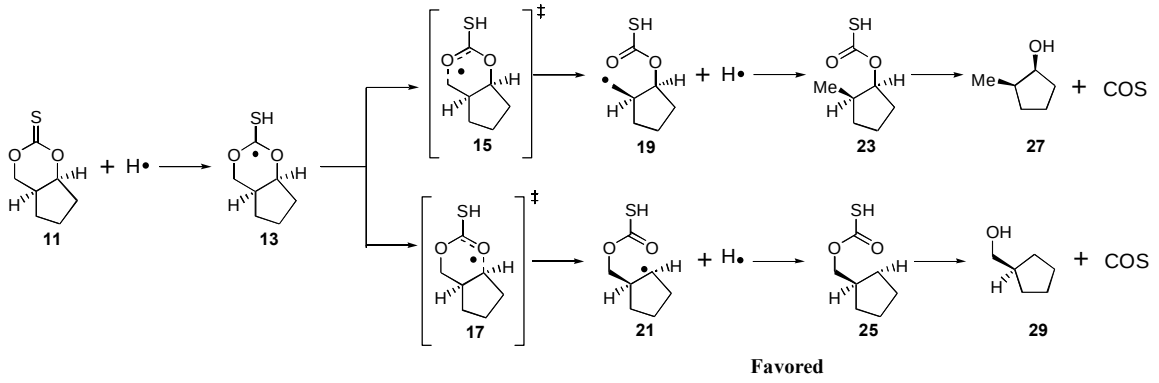

Energy results obtained from the *ab initio* calculations are shown in Figure IV.7. The second column of the table refers to the energy calculated for the compound numbered in the first column. The fourth column represents the energy associated with the complete reaction in each case, *i. e.,* the compound energy plus the value of any extra molecule involved in that reaction step as shown on the third column of the table. The fifth column shows the relative energy for the complete reaction reported in the fourth column converted into Kcal/mol. The graph follows the complete-reaction steps for both the primary and secondary radical paths.

Compd. Number	Energy (Hartree) ab initio		Rxn. Energy (Hartree) ab initio	Rxn. Energy (Kcal/mol) relative
11	-818,1251	H-H	-819,2519	43,6499
13	-818,6578	H•	-819,1560	103,8280
15	-818,6152	H•	-819,1134	130,5599
17	-818,6699	H•	-819,1681	96,2352
19	-818,6884	H•	-819,1867	84,5823
21	-818,6891	H•	-819,1873	84,1807
23	-819,3204		-819,3204	0,6843
25	-819,3145		-819,3145	4,3489
27	-309,0482	COS	-819,3088	7,9195
29	-309,0447	COS	-819,3053	10,1157
H•	-0,4982			
COS	-510,2606			
H-H	-1,1268			

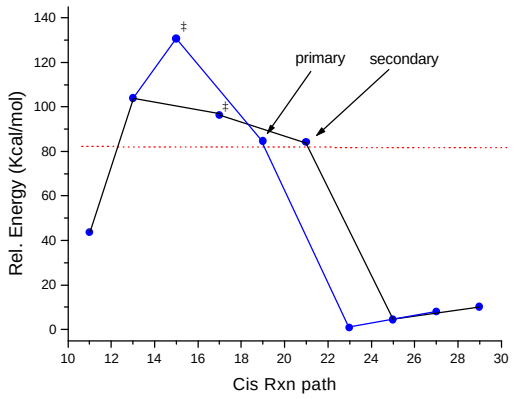

Figure IV.7

Simple thermodynamical analysis would indicate preference for the formation of the secondary radical **21** based on its lower energy as compared to the primary radical **19**. The difference in energy is 6.36 x 10^{-4} Hartree (0.399 Kcal/mol) which gives an approximate 2:1 selectivity at 25^{o} C for formation of the secondary radical. This agrees with what was expected based on stability of secondary *versus* primary radical analysis. This projected 2:1 selectivity[208] value assumes that the formation of the radical is irreversible and thus the rate-determining step. Clearly, this difference in energy is not large enough to justify the selectivity observed experimentally.

Comparison of the difference in energy for the two possible products of the reaction (**27, 29**) gives a difference of 5.8 x 10^{-3} Hartree (3.66 Kcal/mol) favoring formation of the primary product-radical **23**, and 3.5 x 10^{-3} Hartree (2.20 Kcal/mol)

[208] Based on $\Delta G = - RT \ln K$ where R= 1.9872 cal/molK.

favoring the formation of the primary product **27**. This would be the expected result if the fragmentation reaction was reversible.

Both charge and spin distributions are as expected given the atom types and the position of the radicals. The radical was not localized for the transition state **15**; instead it was partially distributed between the thionocarbonate carbon and the emerging carbon radical. For all other species the spin was localized on one carbon.

The cyclic radical **13** adopted the same conformation of the original reagent **11**. The primary radical reaction path (molecules **13** to **27**) evolved through a series of changes in geometry involving different envelope conformations for the five-membered ring. Transition state **15** resembled the geometry of radical **19** (late transition state). The secondary radical reaction path showed similar changes in geometry and a late transition state as well.

Both primary and secondary radicals (**19, 21**) adopted nearly flat conformations, while the cyclic radical **13** is pyramidal. The preferred geometry of tri-coordinated carbon radicals is well known[209], with a planar or nearly planar preferred configuration (around 10^{o} tolerance) with tiny barriers for inversion. Electronegative substituents (oxygen, halogens, etc.) are known to cause a radical to pyramidalize, and raise its barrier to inversion, as was observed for **13**.

Radical reactions usually occur with a transition state that resembles the geometry of the planar radical, a late transition state[209]. The transformation to the planar radical is associated with an increase in bond angles, which reduces the repulsive effects between

---

[209] Ruchardt, C. *Angew. Chem. Int. Ed. Eng.* **1970**, *9*, 830.

substituents. Along the same line, any influence that tends to reduce the angle between the orbitals or bonds encounters strong resistance due to an increase of strain.

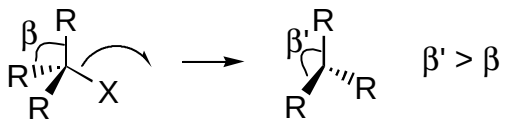

Analysis of the strain associated with angle strain for each molecule was accomplished using the offset-from-the-ideal-angle calculation described in the *ab initio* procedure section of this Addendum. The change in the offset-from-the-ideal-angle associated with the ring portion of the molecule showed an increase for the formation of the radicals (**19**, **21**) leading to both the primary and secondary products (**23**, **25**) as shown in the graphs in Figure IV.8. There was a smaller increase in the offset associated with the formation of the primary radical (**19**). This difference is better demonstrated in the detail graph where the data corresponding to the transition states have been removed for the sake of clarity.

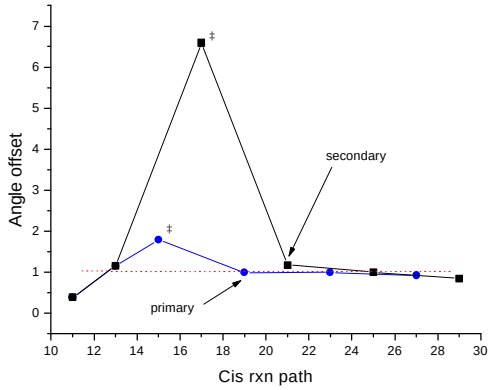

Compound Number	Total Offset	Ring Offset	carbonate Offset
11	0.3847	0.3847	0.2837
13	1.1524	0.3535	0.4543
15	1.7867	0.3979	1.4041
17	6.5950	2.9316	6.0601
19	0.9894	0.4723	
21	1.1768	0.5634	
23	0.9933	0.4667	
25	0.9949	0.3792	
27	0.9197	0.3733	
29	0.8493	0.3352	

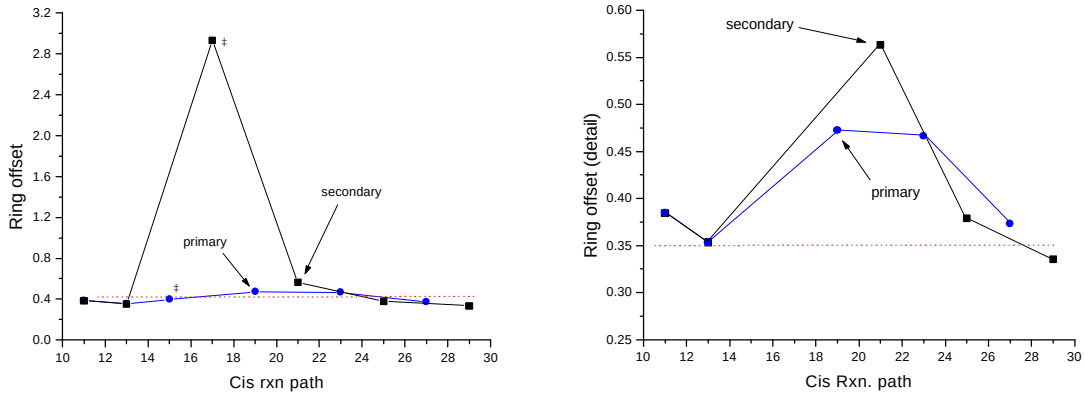

Figure IV.8

Analysis of the offset-from-the-ideal-angle change at each atom position for a specific transition was also considered (see Figure IV.9).

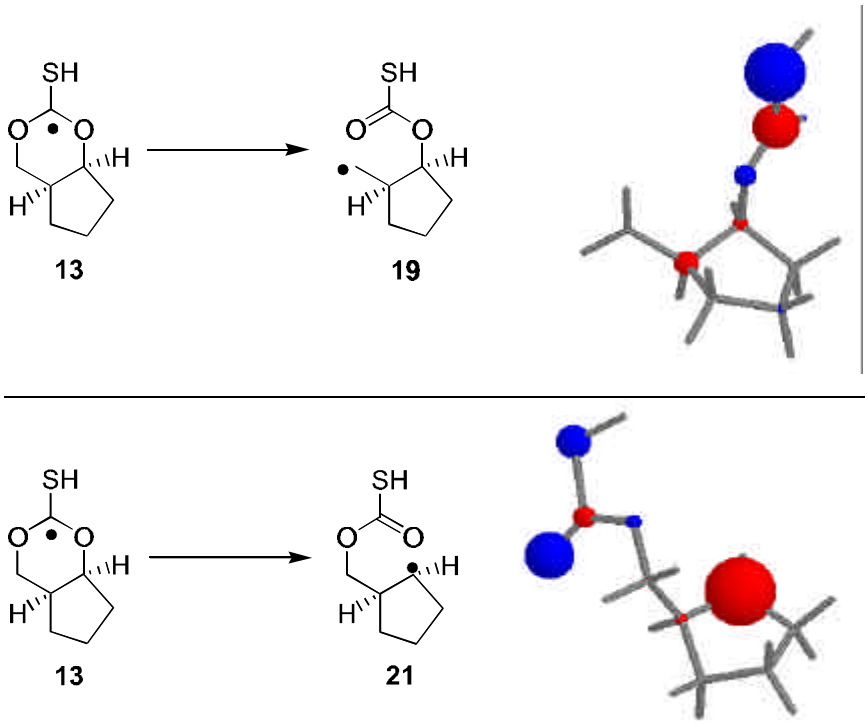

Figure 9: Graphical representation of offset-from-the-ideal-angle change. Red represents an increase in the offset at the indicated position while blue represents a decrease.

Calculation of the change in offset-from-the-ideal-angle for the transformation of cyclic radical **13** into primary radical **19** indicated an increase of ring-offset of 0.12. For the transformation of cyclic radical **13** into secondary radical **21**, the observed change in offset resulted in an increase of ring-offset of 0.21. These values would suggest that formation of the primary radical would be less disfavored due to a smaller increase in the offset and should therefore be the preferred pathway for the reaction. This is not a correct analysis because formation of the secondary radical **21** generates a radical center in the ring, therefore increasing the offset change in the ring for that molecule, while formation of the primary radical **19** does not effect ring-offset. These offset change numbers will be compared instead with the change in offset observed for the trans transformation.

- *Results: Fragmentation reaction - trans:*

The *trans* fragmentation reaction was examined applying similar *ab initio* calculations. The scheme below shows the two possible reaction pathways *via* C-O bond cleavage to give a primary radical (**18**) or a secondary radical (**20**). Experimentally, its been shown that the fragmentation of a *trans* 6-5 system (represented here by compound **12**) gives rise to the product derived from a primary radical (represented here by compound **28**) as the preferred pathway for the reaction (in a ratio of 1:21, see Figure IV.1).

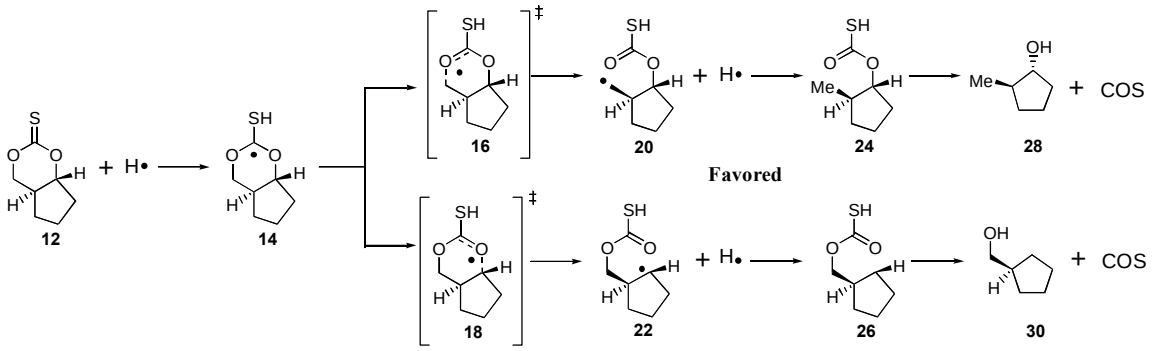

Energy results obtained from the *ab initio* calculations are shown in Figure IV.10. The second column of the table refers to the energy calculated for the compound numbered in the first column. The fourth column represents the energy associated with the complete reaction in each case, *i. e.,* the compound energy plus the value of any extra molecule involved in that reaction step as shown on the third column of the table. The fifth column shows the relative energy for the complete reaction reported in the fourth column converted into Kcal/mol. The graph follows the complete-reaction steps for both the primary and secondary radical paths.

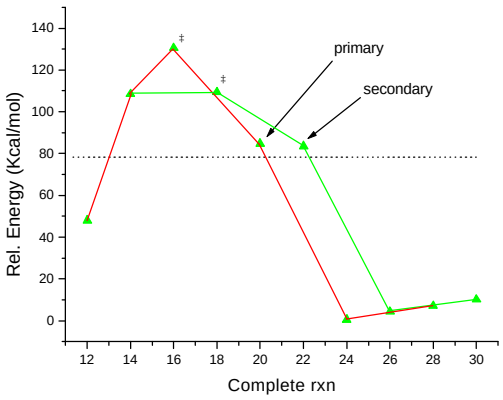

Compd. Number	Energy (Hartree) ab initio		Rxn. Energy (Hartree) ab initio	Rxn. Energy (Kcal/mol) relative
12	-818,1182	H-H	-819,2450	47,9797
14	-818,6504	H•	-819,1486	108,4716
16	-818,6152	H•	-819,1134	130,5599
18	-818,6489	H•	-819,1471	109,4129
20	-818,6881	H•	-819,1863	84,8082
22	-818,6901	H•	-819,1884	83,5281
24	-819,3206		-819,3206	0,5713
26	-819,3145		-819,3145	4,3489
28	-309,0497	COS	-819,3103	7,0033
30	-309,0447	COS	-819,3053	10,1157
H•	-0,4982			
COS	-510,2606			
H-H	-1,1268			

Figure IV.10

Simple thermodynamical analysis would indicate preference for the formation of the secondary radical **22** based on its lower energy as compared to the primary radical **20**, the same behavior observed for the *cis* series. The difference in energy is 2.04 x 10^{-3} Hartree (1.28 Kcal/mol) which gives an approximate 6:1 selectivity[208] at 25° C favoring formation of the secondary radical. This agrees with what was expected based on stability of secondary *versus* primary radical analysis but not with the experimental results obtained for the radical fragmentation of similar compounds. This projected 6:1 selectivity value assumes that the formation of the radical is irreversible and thus the rate-determining step.

Comparison of the difference in energy for the two possible products of the reaction (**28, 30**) gave a difference of 6.0 x 10^{-3} Hartree (3.78 Kcal/mol) favoring formation of the primary product-radical **24** and 5.0 x 10^{-3} Hartree (3.11 Kcal/mol) favoring the formation of the primary product **28**. This would be the expected result if the fragmentation reaction was reversible, but since the reaction is under kinetic control, the stability of the final product should not determine the formation of the final product.

Both charge and spin distributions are as expected given the atom types and the position of the radicals. The radical was not localized for transition state **16**; instead it was partially distributed between the thionocarbonate and the emerging radical carbon. For all other species the spin was localized on one carbon.

The cyclic radical **14** adopted the same conformation as the original reagent **12**. The primary radical reaction pathway evolved through a series of changes in geometry involving the envelope conformation of the five-membered ring. The transition state **16** resembled the geometry of radical **20 (**late transition state). The secondary radical

reaction pathway showed similar changes in geometry, with an early transition state and the spin concentrated in the original thionocarbonate carbon. Both primary and secondary radicals (**20, 22**) were close to flat, while the cyclic radical **14** was pyramidal.

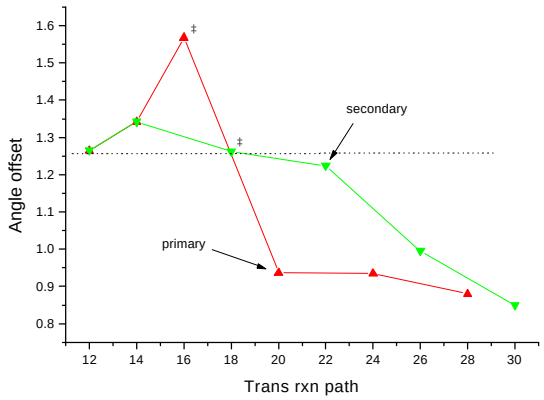

Compound Number	Total Offset	Ring Offset	carbonate Offset
12	1.2646	0.5961	1.0319
14	1.3420	0.5476	0.6243
16	1.5677	0.4528	1.2489
18	1.2623	0.5476	0.8168
20	0.9370	0.4230	
22	1.2241	0.6124	
24	0.9351	0.4144	
26	0.9949	0.3792	
28	0.8803	0.3266	
30	0.8493	0.3352	

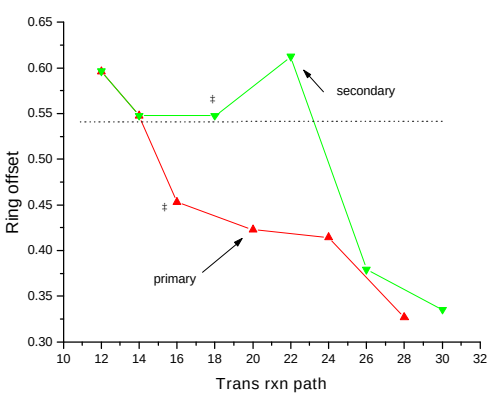

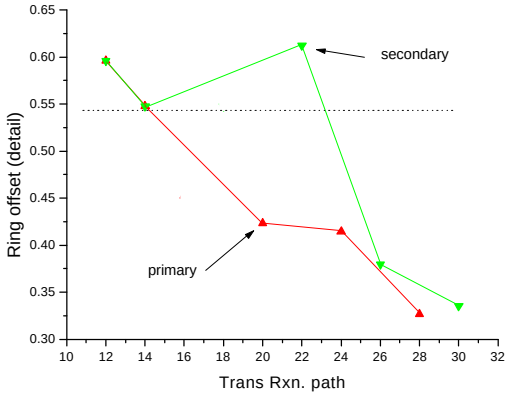

Figure IV.11

Analysis of offset-from-the-ideal-angle associated with each compound showed that formation of the radicals resulted on an increase of ring-offset for the formation of the secondary radical **22** of 0.07 and a release of ring-offset for the formation of primary radical **20** of 0.13. This difference in ring-offset is better demonstrated in the detail graph

where the data corresponding to the transition states have been removed for the sake of clarity (see Figure IV.11).

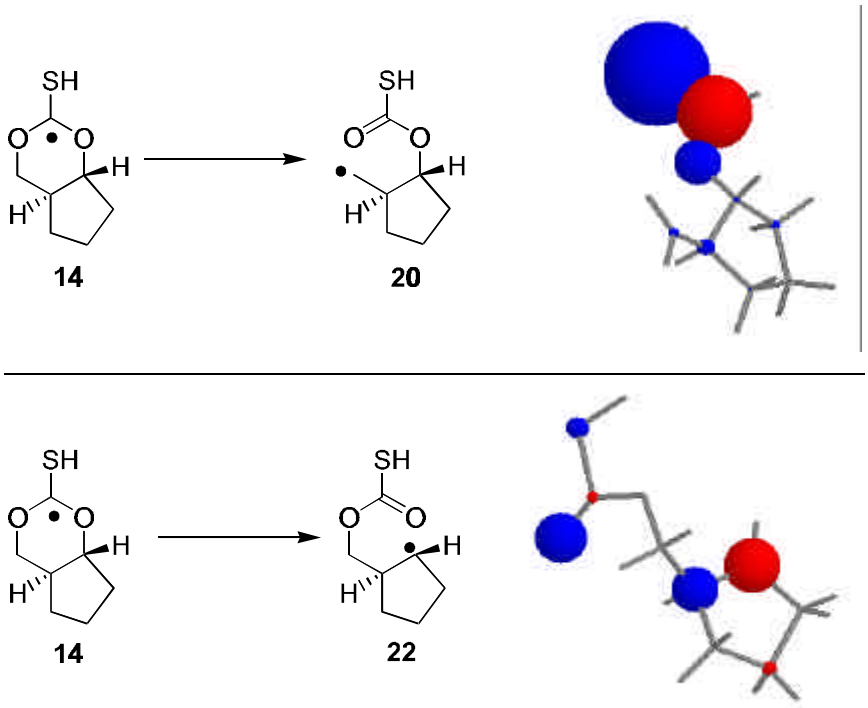

Figure IV.12: Graphical representation of offset-from-the-ideal-angle change. Red represents an increase in angle offset at the indicated position while blue represents a decrease.

Analysis of the change in offset-from-the-ideal-angle at each atom position for a specific transition was considered for the transformation of cyclic radical **14** into primary radical **20** and secondary radical **22** and is illustrated in Figure IV.12. Formation of the primary radical **20** implied in a relief of ring-offset of 0.13 while formation of the secondary radical **22** implied in an increase of the ring-offset of 0.07. These values suggest that formation of the primary radical is favored due to a decrease in ring-offset and should therefore be the preferred pathway for the reaction.

The change in offset observed for the transformation of the *cis* series were compared with the results obtained for the *trans* series. Analysis of the results showed that formation of the primary radical (**19** and **20**) involved increase of the offset for the ring atoms for compound **19** (see Figure 9) and a release of offset for the ring atoms in compound **20** (see Figure 12). For the secondary radical, there was always an increase of the offset associated with the formation of the radical in the ring and therefore it does not play a big role in determining the selectivity of the reaction.

The *trans* series offset is overall laeger than the *cis* series. Under these circumstances release of ring-offset associated with C-O bond cleavage are proportionally more important and thus the offset play a bigger role in defining selectivity towards formation of the primary radical **20** and overcomes the thermodynamical tendencies of the system towards formation of the secondary radical.